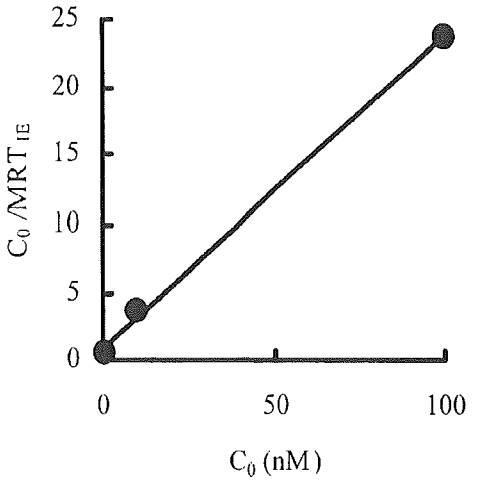

Figure 3. Linear plots of C_0/MRT_{IE} versus C_0. Symbols represent C_0/MRT_{IE} calculated by Equation (2), with lines fitted using Equation (3). *a* and *b*, are parameters described in Equation (3), and were calculated to be 4.35 and 3.47, respectively. r, is the correlation coefficient of linear plots, and was calculated to be 0.999.

the 21-mer siRNA and the 27-mer dsRNA, respectively, indicating that the 27-mer siRNA is only threefold more potent than the conventional one, as far as the total RNAi potency is evaluated by the AUC_{IE}. The MRT_{IE} calculated (3.82 for the 21-mer siRNA and 6.47 for the 27-mer dsRNA) also indicated a moderate increase. These findings strongly suggest that the AUC_{IE} and MRT_{IE} are useful parameters to quantitatively compare the potency of various types of RNAi effectors including ones that will be developed in future.

In conclusion, the AUC_{IE} and MRT_{IE} proposed in this study can be calculated by simple numerical integration. The AUC_{IE} can be used as an index of the intensity of gene silencing effect of siRNA delivered, whereas MRT_{IE} can be used for the duration of the RNAi effect. The time-course of the reduction in protein expression by siRNA was successfully evaluated by the proposed kinetic analysis, thereby providing important parameters to evaluate the extent and duration of gene silencing by siRNA and to quantitatively understand and efficiently control RNAi. Also, these parameters will be useful for predicting the duration of the gene silencing effect of siRNA before applying it as an experimental tool as well as a therapeutic treatment. Moreover, our proposed moment analysis is suitable for designing experimental or therapeutic protocols in which siRNA is administered repeatedly to obtain a sustained gene silencing effect as well as providing well-controlled experimental conditions or a good therapeutic effect.

References

Caplen NJ, Parrish S, Imani F, Fire A, Morgan RA. 2001. Specific inhibition of gene expression by small double-stranded RNAs in invertebrate and vertebrate systems. Proc Natl Acad Sci USA 98:9742–9747. Epub 2001 Jul 31.

Elbashir SM, Harborth J, Lendeckel W, Yalcin A, Weber K, Tuschl T. 2001. Duplexes of 21-nucleotide RNAs mediate RNA interference in cultured mammalian cells. Nature 411:494–498.

Hahn P, Schmidt C, Weber M, Kang J, Bielke W. 2004. RNA interference: PCR strategies for the quantification of stable degradation-fragments derived from siRNA-targeted mRNAs. Biomol Eng 21:113–117.

Haley B, Zamore PD. 2004. Kinetic analysis of the RNAi enzyme complex. Nat Struct Mol Biol 11:599–606. Epub 2004 May 30.

Kim DH, Behlke MA, Rose SD, Chang MS, Choi S, Rossi JJ. 2005. Synthetic dsRNA Dicer substrates enhance RNAi potency and efficacy. Nat Biotechnol 23:222–226. Epub 2004 Dec 26.

McManus MT, Sharp PA. 2002. Gene silencing in mammals by small interfering RNAs. Nat Rev Genet 3:737–747.

Milhavet O, Gary DS, Mattson MP. 2003. RNA interference in biology and medicine. Pharmacol Rev 55:629–648.

Miyagishi M, Hayashi M, Taira K. 2003. Comparison of the suppressive effects of antisense oligonucleotides and siRNAs directed against the same targets in mammalian cells. Antisense Nucleic Acid Drug Dev 13:1–7.

Poste G, Doll J, Hart IR, Fidler IJ. 1980. In vitro selection of murine B16 melanoma variants with enhanced tissue-invasive properties. Cancer Res 40:1636–1644.

Raab RM, Stephanopoulos G. 2004. Dynamics of gene silencing by RNA interference. Biotechnol Bioeng 88:121–132.

Reynolds A, Leake D, Boese Q, Scaringe S, Marshall WS, Khvorova A. 2004. Rational siRNA design for RNA interference. Nat Biotechnol 22:326–330. Epub 2004 Feb 1.

Takahashi Y, Nishikawa M, Kobayashi N, Takakura Y. 2005. Gene silencing in primary and metastatic tumors by small interfering RNA delivery in mice: Quantitative analysis using melanoma cells expressing firefly and sea pansy luciferases. J Control Release 105:332–343.

Tuschl T, Zamore PD, Lehmann R, Bartel DP, Sharp PA. 1999. Targeted mRNA degradation by double-stranded RNA in vitro. Genes Dev 13: 3191–3197.

Yamaoka K, Nakagawa T, Uno T. 1978. Statistical moments in pharmacokinetics. J Pharmacokinet Biopharm 6:547–558.

Yoshinari K, Miyagishi M, Taira K. 2004. Effects on RNAi of the tight structure, sequence and position of the targeted region. Nucleic Acids Res 32:691–699. Print 2004.

Zamore PD, Tuschl T, Sharp PA, Bartel DP. 2000. RNAi: Double-stranded RNA directs the ATP-dependent cleavage of mRNA at 21 to 23 nucleotide intervals. Cell 101:25–33.

THE JOURNAL OF GENE MEDICINE
J Gene Med 2006; **8**: 53–62.
Published online 25 July 2005 in Wiley InterScience (www.interscience.wiley.com). **DOI:** 10.1002/jgm.812

RESEARCH ARTICLE

Use of lipoplex-induced nuclear factor-κB activation to enhance transgene expression by lipoplex in mouse lung

Takeshi Kuramoto[1]
Makiya Nishikawa[2]*
Oranuch Thanaketpaisarn[1]
Takayuki Okabe[1]
Fumiyoshi Yamashita[1]
Mitsuru Hashida[1]

[1]*Department of Drug Delivery Research, Graduate School of Pharmaceutical Sciences, Kyoto University, Sakyo-ku, Kyoto 606-8501, Japan*

[2]*Department of Biopharmaceutics and Drug Metabolism, Graduate School of Pharmaceutical Sciences, Kyoto University, Sakyo-ku, Kyoto 606-8501, Japan*

*Correspondence to:
Makiya Nishikawa, Department of Biopharmaceutics and Drug Metabolism, Graduate School of Pharmaceutical Sciences, Kyoto University, Sakyo-ku, Kyoto 606-8501, Japan. E-mail: makiya@pharm.kyoto-u.ac.jp

Received: 4 September 2004
Revised: 19 April 2005
Accepted: 23 May 2005

Abstract

Background Although lipofection-induced TNF-α can activate nuclear factor κB (NF-κB), which, in turn, increases the transgene expression from plasmid DNA in which any NF-κB responsive element is incorporated, no attempts have been made to use such biological responses as NF-κB activation against a vector to enhance vector-mediated gene transfer.

Methods A lipoplex composed of *N*-[1-(2,3-dioleyloxy)propyl]-*N*,*N*,*N*-trimethylammonium and cholesterol liposome and plasmid DNA encoding firefly luciferase under the control of the cytomegalovirus immediate early promoter (pCMV-Luc) was intravenously injected into mice. Luciferase activity as well as NF-κB activation in the lung were evaluated. Then, a novel plasmid DNA, pCMV-κB-Luc, was constructed by inserting 5 repeats of NF-κB-binding sequences into the pCMV-Luc.

Results NF-κB in the lung was activated by injection of the lipoplex and its nuclear localization was observed. An injection of lipopolysaccharide 30 min prior to the lipofection further activated NF-κB. At the same time, the treatment significantly increased the transgene expression by lipoplex, suggesting a positive correlation between expression and NF-κB activity. Based on these findings, we tried to enhance the lipoplex-based transgene expression by using NF-κB activation. The lipoplex consisting of pCMV-κB-Luc showed a 4.7-fold increase in transgene expression in the lung compared with that with pCMV-Luc.

Conclusions We demonstrated that NF-κB activation by lipoplex can be used to enhance lipoplex-mediated transgene expression by inserting NF-κB-binding sequences into plasmid DNA. These findings offer a novel method for designing a vector for gene transfer in conjunction with biological responses to it.

Keywords lipoplex; TNF-α; NF-κB; lung; plasmid DNA; CMV promoter

Introduction

The cationic liposome/plasmid DNA complex, or lipoplex, is a safe and convenient nonviral vector that has been intensively studied for *in vivo* gene transfer [1–3]. However, it has some drawbacks, such as a low level of transgene expression, which is mainly attributed to the biological barrier preventing exogenous plasmid DNA passing through biological membranes such as the plasma and endosomal membranes, and the nuclear envelope [4,5]. The use of dioleoyl phosphatidylethanolamine (DOPE) as a helper

lipid in cationic liposome formulations can improve the delivery of plasmid DNA into the cytoplasm through destabilization of the endosomal membrane, leading to increased transgene expression. Intratracheal or intratissue gene transfer using lipoplex formulated with DOPE-containing cationic liposomes has been shown to be very efficient. However, such lipoplexes induce fusion of erythrocytes and produce less transgene expression after systemic administration [6].

Another drawback is the nonspecific and systemic production of inflammatory cytokines such as tumor necrosis factor (TNF)-α, interferon (IFN)-γ and interleukin (IL)-12, mostly induced by the unmethylated CpG motif contained in plasmid DNA [7–9]. Kupffer cells in the liver are the major source of these cytokines after intravenous injection of lipoplex [10]. Excessive production of such cytokines can be regarded as a side effect of lipofection and should be reduced as much as possible. Various approaches have been designed to decrease cytokine production, including a reduction in the number of immunostimulatory CpG motifs [11], the use of PCR-amplified DNA fragments [12], and sequential injection of cationic liposomes and plasmid DNA [13].

On the other hand, biological responses such as cytokine production may be used to enhance the transgene expression by lipoplex. Of the cytokines induced by lipoplex, TNF-α is a well-known activator of the transcription factor nuclear factor κB (NF-κB) that is present in the cytoplasm of a variety of cells [14–16]. Upon activation NF-κB translocates and accumulates in the nucleus, binds to its recognition DNA element, and participates in the activation of transcription of various genes [17]. Genes activated by NF-κB include cell-surface molecules such as immunoglobulin κ light chain, class I and II major histocompatibility complex, and various cytokines. In addition, some viruses including cytomegalovirus (CMV) have also NF-κB-binding sites in their enhancers, and viral production is stimulated by agents that activate NF-κB [18].

These pieces of evidence have led us to form a hypothesis that lipofection-induced TNF-α activates NF-κB in target cells, which, in turn, increases the transgene expression from plasmid DNA in which any NF-κB-responsive element is incorporated. However, no attempts have been made to use such biological responses as NF-κB activation against a vector to enhance vector-mediated gene transfer. In the present study, therefore, we first investigated whether NF-κB in the lung was activated after intravenous injection of a lipoplex. Plasmid DNA encoding firefly luciferase under the control of CMV immediate early promoter (pCMV-Luc) was used as a model plasmid, and *N*-[1-(2,3-dioleyloxy)propyl]-*N*,*N*,*N*-trimethylammonium (DOTMA) and cholesterol (Chol) liposomes (DOTMA/Chol liposomes) were prepared as cationic liposomes. To examine the correlation between NF-κB activation and transgene expression, we examined the effect of lipopolysaccharide (LPS), a well-known activator of NF-κB, and found a positive correlation between the activation and transgene expression in the lung. Based on these findings, we constructed a novel plasmid DNA, pCMV-κB-Luc, by inserting 5 additional NF-κB-binding sequences into the pCMV-Luc, and achieved significantly enhanced transgene expression in the lung by intravenous injection of a lipoplex containing the novel plasmid DNA.

Materials and methods

Chemicals

DOTMA was purchased from Tokyo Kasei (Tokyo, Japan). Chol was purchased from Nacalai Tesque (Kyoto, Japan). LPS was purchased from Sigma (St. Louis, MO, USA). ^{111}Indium chloride was supplied by Nihon Medi-Physics Co. (Takarazuka, Japan). [γ-^{32}P]ATP was purchased from Amersham (Tokyo, Japan). PathDetect® NF-κB *cis*-reporting pNF-κB-Luc plasmid was purchased from Stratagene (La Jolla, CA, USA). Opti-MEM I was obtained from Gibco BRL (Grand Island, NY, USA). The nuclear extract kit was supplied from Active motif. Oligonucleotides were purchased from Sawady (Tokyo, Japan); one with a NF-κB-binding sequence (5′-TCAGAGGGGACTTTCCGAGAGG-3′, the underlined part represents the NF-κB-binding sequence) and one with a random sequence (5′-AGTGTCAGCACGTGGAGATGCG-3′) were used. All other chemicals were of the highest purity available.

Plasmid DNA

pCMV-Luc was constructed by inserting the *Hind*III/*Xba*I firefly luciferase cDNA fragment from pGL3-control vector (Promega, Madison, WI, USA) into the *Hind*III/*Xba*I site of pcDNA3 vector (Invitrogen, Carlsbad, CA, USA) as previously reported [6]. pCMV-κB-Luc was constructed by inserting the *Bgl*II/*Nru*I site of the 5 repeats of the NF-κB-binding sequence from pNF-κB-Luc into the *Bgl*II/*Nru*I site of pCMV-Luc. Each plasmid DNA was amplified in the *E. coli* strain DH5α and then isolated and purified using a Qiagen Endofree™ Plasmid Giga kit (Qiagen GmbH, Hilden, Germany). The LPS concentration in plasmid DNA was measured with a LAL assay kit (Limus F Single Test Wako; Wako Pure Chemical, Osaka, Japan) and found to be less than 22 pg/μg DNA. Then purified plasmid DNA was dissolved in sterilized endotoxin-free 5% dextrose and stored at −20 °C until required.

Preparation of cationic liposomes

A mixture of 15.2 mg DOTMA and 8.8 mg Chol in 12 ml chloroform was dried as a thin film, vacuum desiccated, and hydrated with vortexing in 3 ml sterilized 5% dextrose to give a final concentration of 3.5 mg DOTMA/ml in a 50-ml round-bottomed flask [10]. After hydration, the dispersion was sonicated for 3 min in a bath sonicator at

37 °C. The lipid solution was frozen in liquid nitrogen for 2 min and thawed in a water bath for 6 min at 37 °C. The dispersion was passed through a MILLEX®-GV 0.22 μm filter unit (Millipore, Bedford, MA, USA). The particle size of the cationic liposomes was found to be about 160 nm by dynamic light scattering spectrophotometry (LS-900, Otsuka Electronics, Osaka, Japan). The lipid concentration was determined by the Cholesterol C-II Test Wako (Wako Pure Chemical, Osaka, Japan).

Preparation of lipoplex

The liposome dispersion (4.5 mg/ml) was diluted to 1.25 mg/ml and 2 mg plasmid DNA/ml solution were diluted with 5% dextrose to 0.25 mg/ml. An equal volume of each diluted solution was mixed in a water bath at 37 °C and allowed to stand for 30 min. The particle size of the lipoplex was measured in 5% dextrose and found to be about 250 nm in diameter.

Animal experiments

Male ddY and male BALB/c mice were purchased from the Shizuoka Agricultural Co-operative Association for Laboratory Animals (Shizuoka, Japan) and maintained on a standard food and water diet under conventional housing conditions. All animal experiments were conducted in accordance with the principles and procedures outlined in the National Institutes of Health Guide for the Care and Use of Laboratory Animals. The protocols for animal experiments were approved by the Animal Experimentation Committee of the Graduate School of Pharmaceutical Sciences of Kyoto University.

Tissue distribution after intravenous injection of lipoplex

Plasmid DNA (pCMV-Luc) was radiolabeled with ^{111}In as reported elsewhere [19]. Then ^{111}In-plasmid DNA was diluted with nonradiolabeled plasmid DNA to give a dose of plasmid DNA of 25 μg/mouse. Male ddY mice (20–22 g) received the lipoplex containing ^{111}In-plasmid DNA in sterilized 5% dextrose by tail vein injection. Mice were killed at 1, 10, 60 and 120 min after injection and the liver, kidney, spleen, lung, and heart were harvested, rinsed with saline and weighed. Blood was withdrawn from the vena cava and urine was collected from the bladder. The ^{111}In-radioactivity of the samples was counted in a well-type scintillation counter (ARC-500, Aloka, Tokyo, Japan).

In vivo transfection and reporter gene assay

Male BALB/c mice (20 g) received lipoplex at a dose of 25 μg plasmid DNA/mouse in 200 μl 5% dextrose by tail vein injection. At indicated times after injection, the lung was harvested, washed with ice-cold saline, and homogenized with 4 ml/g tissue of lysis buffer (0.1 M Tris, 0.05% Triton X-100, 2 mM EDTA, pH 7.8), and subjected to three cycles of freezing in liquid nitrogen for 3 min and thawing in a water bath at 37 °C for 3 min. The homogenates were centrifuged at 10 000 *g* for 8 min at 4 °C. Then, 10 μl of the supernatant were mixed with 100 μl luciferase assay buffer (Pikkagene, Toyo Ink, Tokyo, Japan) and the chemiluminescence was measured with a luminometer (Lumat LB 9507, EG&G Bethhold, Bad Wildbad, Germany).

Separately, naked plasmid DNA dissolved in a 1.6 ml saline was injected into the tail vein of mice within 5 s at a dose of 1 μg plasmid DNA/mouse [20]. At 6 h after injection, the lung and liver were excised and the luciferase activity was assayed as above.

Cytokine assay

The levels of TNF-α in serum after intravenous injection of the lipoplex were measured using an ELISA kit (AN'ALYZA™, Genzyme, Cambridge, MA, USA) as described previously [21]. Blood was collected into plastic tubes from the vena cava of mice under anesthesia, and allowed to stand for 3 h at 4 °C. Then the samples were centrifuged at 3000 *g* for 30 min at 4 °C and the serum obtained was used for the assay.

Preparation of nuclear protein extracts

Mice were killed at the indicated times after injection of the lipoplex and the lungs were immediately harvested and frozen in liquid nitrogen. Nuclear protein extracts were prepared as described previously [22]. In brief, each lung was immersed in 1 ml of ice-cold lysis buffer (10 mM Hepes, pH 7.9, 10 mM KCl, 1.5 mM $MgCl_2$, 0.5 mM DTT, 0.5 mM PMSF, 2 μg/ml pepstatin A, 2 μg/ml leupeptin, 2 μg/ml L-leucinethiol) and homogenized on ice with a Potter homogenizer. It was then incubated on ice for 15 min and 25 μl of 10% Nonidet P-40 (Sigma Aldrich Japan, Tokyo, Japan) were added. After vortexing for 15 s, the samples were incubated on ice for 20 min and centrifuged at 10 000 *g* for 15 min at 4 °C. The pelleted nuclei were resuspended in 100 μl of extraction buffer (20 mM Hepes, pH 7.9, 420 mM NaCl, 1.5 mM $MgCl_2$, 0.2 mM EDTA, 0.5 mM DTT, 0.5 mM PMSF, 2 μg/ml pepstatin A, 2 μg/ml leupeptin, 2 μg/ml L-leucinethiol) and incubated on ice for 30 min. The nuclear suspension was centrifuged at 10 000 *g* for 15 min at 4 °C to collect the supernatant containing nuclear protein extracts. The concentration of nuclear protein in the resulted supernatant from each lung extract was determined with the Protein Quantification Kit-Wide range (Dojindo Molecular Technologies, Inc., Kumamoto, Japan). Separately, colon26 cells were treated with 4 μM phenazine methosulfate to activate NF-κB, and nuclear

protein extracts from the cells were collected using a nuclear extract kit (Active motif, CA, USA), which were used for the comparison of plasmid DNA in the binding strength to activated NF-κB.

Electrophoretic mobility shift assay (EMSA)

EMSA was performed as described previously [23]. A single-stranded oligonucleotide containing an NF-κB-binding sequence (5′-TCAGAGGGGACTTTCCGAGAGG-3′) was end-labeled with [γ-^{32}P]ATP using polynucleotide kinase T4 (MEGALABEL™, Takara Bio Inc., Otsu, Japan). The end-labeled probe was purified from unincorporated [γ-^{32}P]ATP using Sephadex G-50 (Pharmacia, Uppsala, Sweden) and recovered in TNE buffer (10 mM Tris HCl, 0.1 M NaCl, 1 mM EDTA, pH 7.5). An aliquot of 50 μg extracted nuclear protein was incubated with 15 μl binding buffer (20 mM Hepes, pH 7.9, 0.5 mM EDTA, pH 8.0, 50 mM KCl, 10% glycerol, 0.5 mM DTT, 0.5 mM PMSF) and 2 μg salmon sperm DNA for 15 min on ice. Then 1×10^5 cpm of the radiolabeled oligonucleotide was added to the sample followed by an additional 30 min incubation at room temperature and 2 μl 0.1% bromphenol blue dye were added to each sample. An aliquot of 25 μl of the resulting solution was electrophoresed on a 4% nondenaturing polyacrylamide gel for 75 min at 150 V in TGE buffer. After completion of the electrophoresis, the gel was transferred to a piece of blotting paper and dried under vacuum. The dried gel was exposed to an Imaging Plate (Fuji Photo Film, Kanagawa, Japan) and analyzed by a Bio-Image analyzer system (BAS-2500, Fuji Photo Film).

Competitive EMSA

To compare the binding strength of plasmids with NF-κB, a competitive EMSA was carried out. An aliquot of 60 μg extracted nuclear protein from phenazine methosulfate treated colon26 cells was incubated with the 1.5×10^6 cpm of radiolabeled oligonucleotide on ice for 30 min with varying amounts of pCMV-Luc or pCMV-κB-Luc (0–0.3 μg/sample) in binding buffer as above. Then the samples (20 μl) were electrophoresed on a 4% nondenaturing polyacrylamide gel for 90 min at 150 V in a cold room. After completion of the electrophoresis, the gel was exposed as above and analyzed by a Bio-Image analyzer system (BAS-3000, Fuji Photo Film).

In vitro transfection and reporter gene assay

Cultured ECV304 cells were seeded at 2×10^5 cells per well onto 12-well plates 24 h before transfection. The cells were about 80% confluent at the time of transfection. Then, the cells were incubated with 1 ml Opti-MEM I containing 0.5 μg plasmid DNA complexed with DOTMA/Chol liposome for 4 h. Then the cells were incubated with or without TNF-α (25 ng/ml) for 3 h. After an additional 8 h incubation, the cells were scraped off the plates and centrifuged at 3000 *g* for 3 min at 4 °C. The pellets were resuspended in 1 ml phosphate-buffered slaine (PBS(-)) and subjected to three cycles of freezing and thawing. Aliquots of the supernatant were used to determine the luciferase activity with a luminometer as described above.

Separately, the cells were treated with the lipoplex for 2 h as described above. Then the cells were mixed with 2′,7′-dichlorodihydrofluorescein diacetate (Molecular Probes, Eugene, OR, USA), incubated for 30 min in 5% CO_2, humidified air at 37 °C, and examined under confocal microscopy. Once reactive oxygen species (ROS) were produced, a fluorescent product was generated.

Statistical analysis

The results are given as mean ± standard deviation (SD). Statistical analysis was performed using an unpaired *t*-test. For multiple comparison (Figure 3B), analysis of variance with subsequent Dunnett test was employed to determine the significance of differences. Values of $P < 0.05$ were considered statistically significant.

Results

Tissue distribution of lipoplex and serum TNF-α concentration

Luciferase activity in the lung peaked at 6–12 h after injection, then gradually decreased, showing a transient profile of transgene expression as reported previously (data not shown) [10,24]. Figure 1A shows the time-course of ^{111}In-radioactivity in the blood, liver, and lung after intravenous injection of a lipoplex prepared with DOTMA/Chol liposomes and ^{111}In-labeled plasmid DNA. As described previously [25], the lipoplex rapidly accumulated in the lung and then disappeared from the lung and was mainly delivered to the liver. Using the ^{111}In-labeling technique, the tissue distribution of the lipoplex can be traced longer than before, and it was shown that about 8% of the injected radioactivity remained in the lung at 6 h post-injection. About 50% of the injected radioactivity accumulated in the liver as early as 1 h after injection of the lipoplex. Previous studies in our laboratory showed that liver nonparenchymal cells are mainly involved in this uptake of lipoplex [26] and Kupffer cells in the liver are responsible for the production of TNF-α [10].

Figure 1B shows the time-course of the serum concentration of TNF-α after injection of the lipoplex. TNF-α could be detected as early as 1 h after injection, reaching a peak at 2 h with a value of more than 500 pg/ml, and

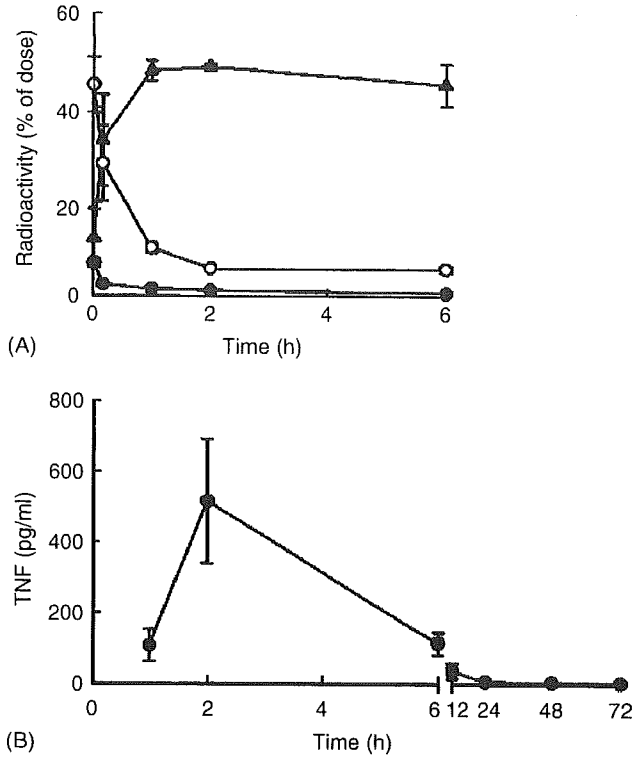

Figure 1. Tissue distribution of radioactivity after intravenous injection of ^{111}In-labeled lipoplex and serum concentration of TNF-α after intravenous injection of lipoplex in mice. (A) Mice received a DOTMA/Chol liposome-^{111}In-plasmid DNA complex at a dose of 25 μg plasmid DNA/mouse. Then blood concentration (●) and tissue accumulation in liver (▲) and lung (○) of radioactivity were determined at the indicated times. The results are expressed as the mean ± SD of three mice. (B) Time course of the serum concentrations of TNF-α after intravenous injection of the lipoplex at a dose of 25 μg plasmid DNA/mouse. At the indicated times post-injection, mice were killed and blood was collected. Serum concentrations of TNF-α were determined by ELISA. The results are expressed as the mean ± SD of three mice

then declining thereafter. At 24 h post-injection, TNF-α was barely detectable in serum.

NF-κB activation in mouse lung after intravenous injection of lipoplex

Activation of NF-κB was detected by an electrophoretic mobility shift assay (EMSA). Mouse lung was collected and homogenized, and the nuclear fractions were subjected to electrophoresis using ^{32}P-labeled oligonucleotide having an NF-κB-binding sequence. No NF-κB was found in the nuclear fraction of the lung from a control mouse (Figure 2, lane 1). On the other hand, NF-κB could be detected in the nuclear fraction of the lung 1 h after intravenous injection of the lipoplex into mice (Figure 2, lanes 2, 3), indicating that the lipoplex activates NF-κB in the lung. The amount of NF-κB detected was greater in mice receiving intravenous LPS 30 min prior to lipofection (Figure 2, lane 4).

The band was reduced by the addition of a 100-fold excess of oligonucleotide having an NF-κB-binding

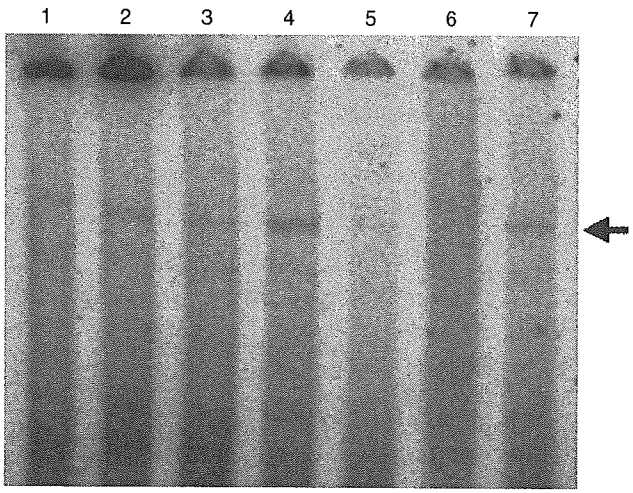

Figure 2. EMSA analysis of NF-κB in mouse lung after intravenous injection of lipoplex. Lane 1: Lung was harvested from untreated mice and nuclear protein extracts were analyzed by EMSA as a negative control. Lanes 2, 3: A pair of mice each received the lipoplex intravenously. One hour after injection, lungs were harvested and nuclear protein extracts were analyzed. Lane 4: Mice received 200 μg LPS 30 min before injection of the lipoplex. One hour after injection, lungs were harvested and nuclear protein extracts were analyzed. Lane 5: The sample from lane 4 was electrophoresed with a 100-fold excess of unlabeled oligonucleotide with an NF-κB-binding sequence. Lane 6: The sample from lane 4 was electrophoresed with a 100-fold excess of pCMV-Luc. Lane 7: The sample from lane 4 was electrophoresed with a 100-fold excess of unlabeled oligonucleotide with a random sequence

sequence to the nuclear extracts from the lipoplex-treated mice (Figure 2, lane 5), not by the addition of a random oligonucleotide (Figure 2, lane 7). These findings support the hypothesis that the band observed is specific to NF-κB. The addition of pCMV-Luc also resulted in disappearance of the band (Figure 2, lane 6). Therefore, this clearly shows that NF-κB binds to pCMV-Luc, probably through the NF-κB-binding sequences existing in the plasmid DNA. So far, it has been observed that NF-κB is activated in the lung by an intravenous injection of the lipoplex, and the activated NF-κB in the lung could affect the transgene expression in the organ.

Enhanced transgene expression through further activation of NF-κB by LPS

To investigate the relationship between the transfection efficiency and NF-κB activation in the lung, we examined the effect of the administration of LPS on transgene expression by the lipoplex. LPS was injected to exaggerate use for NF-κB activation in the lung. Mice receiving 200 μg LPS 30 min prior to the injection of the lipoplex showed a significantly greater transgene expression in the lung than those pre-injected with saline (Figure 3A). Next, LPS was injected after the injection of the lipoplex with different intervals between the injections. The injection of LPS after the lipoplex was also as effective as the

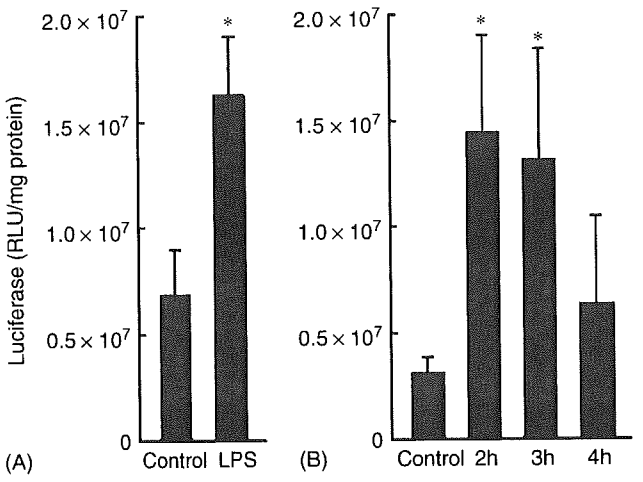

Figure 3. Luciferase activity in lung after intravenous injection of the lipoplex into mice receiving LPS pre- or post-injection. (A) At 30 min before injection of the lipoplex, mice received saline (control) or 200 μg LPS. At 6 h post-injection, mice were killed and the lungs were harvested for luciferase assay. (B) Mice received 200 μg LPS at the indicated times post-intravenous injection of the lipoplex. At 6 h post-injection, mice were killed and the lungs were harvested for luciferase assay. The results are expressed as the mean ± SD of four mice. *$P < 0.05$ vs. the control group

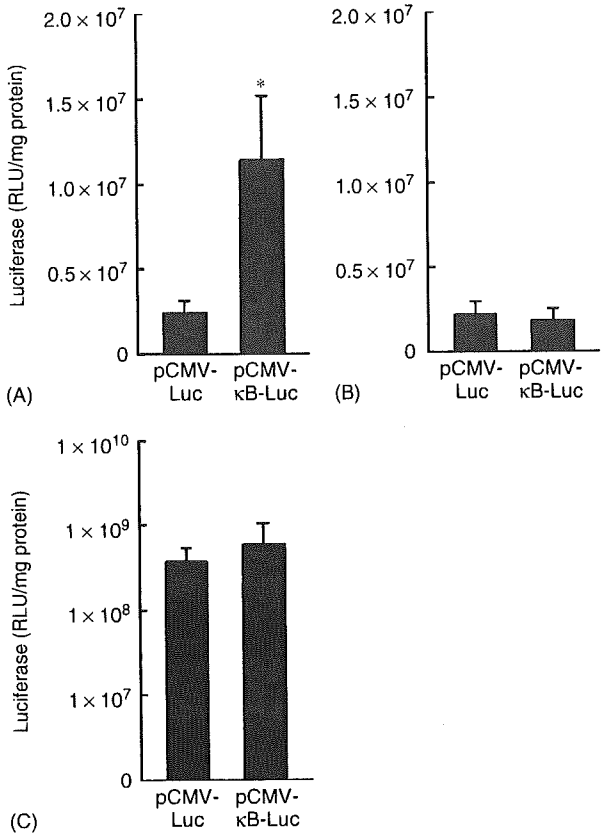

Figure 4. Luciferase activity in mouse lung by pCMV-Luc or pCMV-κB-Luc. (A) Each group of mice received a lipoplex composed of the indicated plasmid DNA at a dose of 25 μg DNA/mouse. At 6 h post-injection, mice were killed and the lungs were harvested for luciferase assay. The results are expressed as the mean ± SD of five mice. (B, C) Each group of mice received a large volume of saline containing the indicated plasmid DNA at a high velocity at a dose of 1 μg DNA/mouse. At 6 h post-injection, mice were killed and the lungs (B) and liver (C) were harvested for luciferase assay. The results are expressed as the mean ± SD of three mice

pre-injection method when the interval was 2 or 3 h (Figure 3B). However, injections at a 4 h interval did not significantly increase the expression. Together with the results of NF-κB activation by LPS (Figure 2, lane 4), these findings suggest that there should be a positive correlation between transgene expression and activation of NF-κB in the lung.

Enhanced transgene expression by lipoplex containing pCMV-κB-Luc

Taking the results of Figures 2 and 3 into consideration, we hypothesized that transgene expression by lipoplex is enhanced by use of activated NF-κB in the lung. Based on this, a novel plasmid vector, pCMV-κB-Luc, was constructed by inserting 5 repeats of an NF-κB-binding sequence upstream of the CMV promoter in pCMV-Luc, on the assumption that the inserted NF-κB-binding sequences would increase the opportunity of plasmid DNA interacting with the transcription factor. A lipoplex prepared with pCMV-κB-Luc showed a significantly greater (4.7-fold, $P < 0.05$) transgene expression in the lung after intravenous injection than that with pCMV-Luc (Figure 4A). Separately, naked plasmid DNA was injected into mice in a large volume of saline at a high velocity, a method which has proved a very powerful method for *in vivo* gene transfer to internal organs [20]. This procedure of gene transfer did not activate NF-κB in the lung (data not shown). Transgene expression by naked pCMV-κB-Luc was as great as that by naked pCMV-Luc in lung and liver (Figures 4B and 4C).

Transgene expression into cultured cells was also examined using ECV304 cells (Figure 5). Cells transfected with pCMV-κB-Luc showed a significantly greater transgene expression (2.14-fold, $P < 0.05$) than ones with pCMV-Luc. In addition, transgene expression by lipoplex containing pCMV-κB-Luc was further increased by the addition of TNF-α (Figure 5). Then, we measured the production of reactive oxygen species (ROS) in the cells. ECV304 cells were treated with the lipoplex for 2 h, then mixed with 2′,7′-dichlorodihydrofluorescein diacetate. We found that the addition of the lipoplex to the cells increased the fluorescent intensity in the cells, the indicator of intracellular ROS, another activator of NF-κB (Figure 6). The addition of the lipoplex induced intracellular ROS in other types of cells including a mouse macrophage cell line, RAW264.7 cells (data not shown).

Binding of NF-κB to pCMV-Luc and pCMV-κB-Luc

To confirm the stronger binding of pCMV-κB-Luc to NF-κB, a competitive EMSA was carried out (Figure 7).

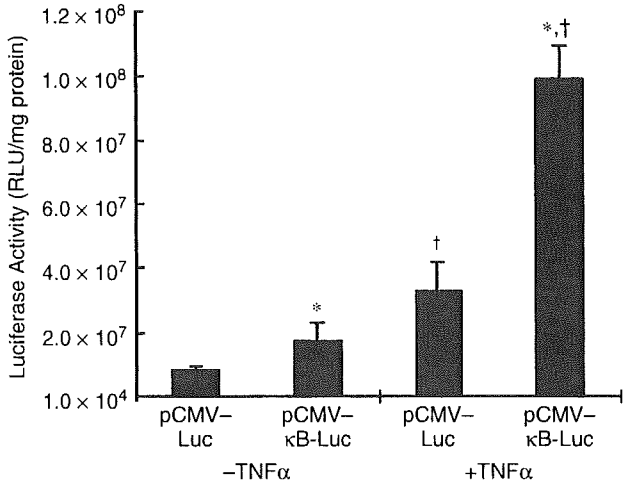

Figure 5. Luciferase activity in ECV304 cells by pCMV-Luc or pCMV-κB-Luc. ECV304 cells were transfected with a lipoplex consisting of the indicated plasmid DNA at a dose of 0.5 μg DNA/well for 4 h. TNF-α was added at a final concentration of 25 ng/ml and incubated for 3 h. After an additional 8 h of incubation, the luciferase activity was measured. The results are expressed as the mean ± SD of three wells. *$P < 0.05$ vs. pCMV-Luc group and †$P < 0.05$ vs. each control (without TNF-α treatment) group

Both pCMV-Luc and pCMV-κB-Luc reduced the specific binding of the radiolabeled probe to the nuclear extracts in a concentration (amount)-dependent manner. However, the reduction was more intense when pCMV-κB-Luc was added to the sample mixture. These results clearly demonstrate that pCMV-κB-Luc has greater binding ability with NF-κB than pCMV-Luc.

Discussion

Lipoplex-based transgene expression is considerably lower than that obtained with viral vectors. This can be explained by the fact that there are many biological barriers obstructing the access of plasmid DNA to the nucleus *in vivo* [27]; nucleases in the systemic circulation, the tangled structure of the extracellular matrix, degradation in the endosomes/lysosomes, and passage through the endosomal membrane and nuclear envelope. Some studies have investigated the physicochemical properties of lipoplex, and lipid composition of cationic liposomes has been optimized to overcome such barriers [28,29]. On the other hand, Zabner *et al.* [5] reported that the nuclear envelope is the main obstacle to lipofection. However, the details of the nuclear translocation of plasmid DNA are still unclear. Plasmid DNA is unlikely to passively diffuse into the nucleus, because its molecular size (usually <2000 kDa) is much greater than the passive diffusion limit (40–60 kDa) [30]. Some researchers reported that plasmid DNA is translocated into the nucleus through the nuclear pore complex (NPC) [31]. Macromolecules that use the NPC pathway have to be provided with a nuclear localization signal (NLS). However, plasmid DNA does not have any such signals, so this suggests that there may be a certain substance that provides plasmid DNA with a NLS. Dean *et al.* [31,32] reported that cytoplasmically microinjected plasmid DNA is translocated into the nucleus in association with several types of transcription factors (SP1, AP1, AP2, Oct-1, etc.). Such transcription factors bind to their corresponding sequences in plasmid DNA, and the transcription factor-associated plasmid DNA is translocated into the nucleus through the NPC. In the present study, we used a plasmid DNA, pCMV-Luc, that contains the CMV promoter, which has been reported to have 4 repeats of the NF-κB-binding sequences [33]. Therefore, it is possible that pCMV-Luc can be translocated into the nucleus through the activation of NF-κB. Mesika *et al.* [34] reported the NF-κB-assisted import of plasmid DNA into the nuclei of mammalian cells *in vitro*.

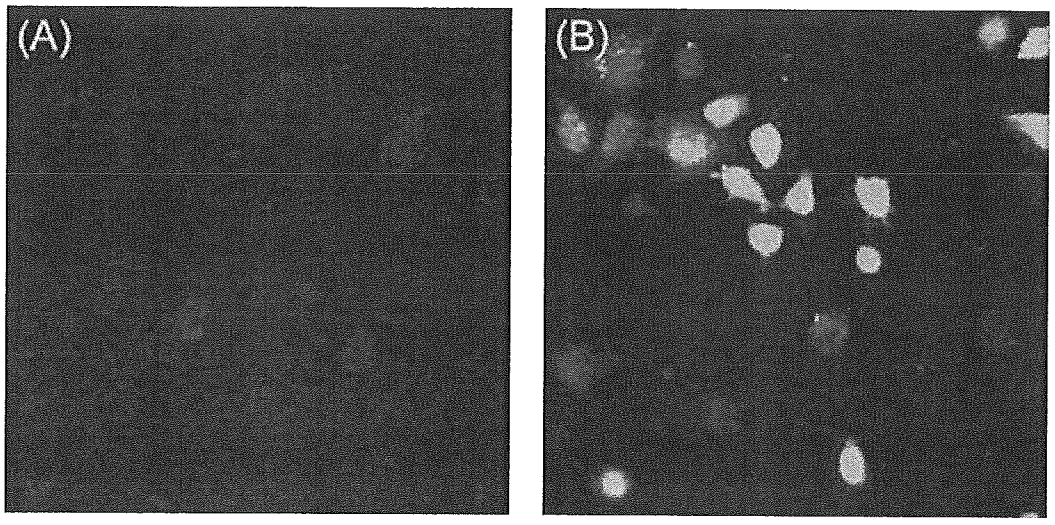

Figure 6. Confocal microscopic images of ECV304 cells treated with lipoplex. The cells were incubated with (B) or without the lipoplex (A, control) for 2 h and mixed with 2′,7′-dichlorodihydrofluorescein diacetate. Then, the cells were incubated for 30 min at 37 °C, and observed by confocal microscopy

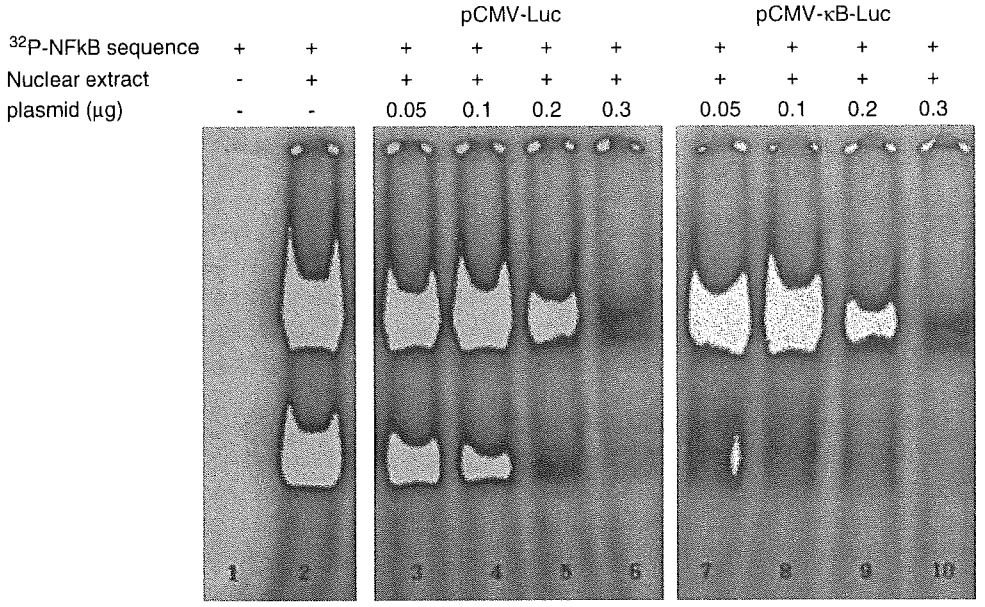

Figure 7. Inhibition of the binding of radiolabeled NF-κB concensus oligonucleotide with nuclear extracts by pCMV-Luc and pCMV-κB-Luc. Extracted nuclear protein from colon26 cells treated with phenazine methosulfate was incubated with the radiolabeled oligonucleotide with varying amounts of pCMV-Luc or pCMV-κB-Luc. Then the samples were electrophoresed on a 4% nondenaturing polyacrylamide gel for 90 min at 150 V in a cold room. After completion of the electrophoresis, the gel was exposed as above and analyzed by a Bio-Image analyzer system (BAS-3000, Fuji Photo Film)

In agreement with previous reports, our investigations showed that transgene expression was transient and greatest in the lung after intravenous injection of the lipoplex (data not shown). Intravenously injected lipoplexes became aggregated with erythrocytes or serum protein and entrapped in the capillaries of the lung, the first-pass organ after intravenous injection [25,35]. Most transgene expression occurred in the endothelial cells in this organ. In this study, we clearly demonstrated that only 8% of the injected lipoplex remained in the lung after intravenous injection and about 50% was delivered to the liver. The newly developed residualizing radiolabel [19] enabled us to trace the tissue distribution of the lipoplex for a much longer period after injection.

The fraction delivered to the liver was reported to be responsible for the production of inflammatory cytokines [10]. A significant level of TNF-α was observed in the serum after intravenous injection of the lipoplex. Serum TNF-α could be detected as early as 1 h after injection and peaked at 2 h then gradually diminished. Several reports claim that the production of TNF-α is mainly attributed to the unmethylated CpG motif contained in plasmid DNA [7–9]. Although several cytokines are produced by lipofection, we focused on TNF-α for the following reasons: (1) TNF-α is secreted primarily by macrophages recognizing a foreign substrate such as CpG motifs in plasmid DNA and IFN-γ or IL-12 are secreted thereafter [24]; (2) TNF-α plays a major role in cytokine-mediated cytotoxicity; and (3) TNF-α is one of the most potent stimulators of NF-κB [14–16]. In this study, we demonstrated that an injection of lipoplex activates NF-κB in the lung, the target organ for gene transfer (Figure 2, lanes 2, 3). To our knowledge, this is the first report showing that lipoplex activates NF-κB in the lung following administration. TNF-α secreted in the circulation should be involved in this activation. In addition to this pathway, the lipoplex might activate NF-κB by a direct pathway via an electrostatic interaction with the cell membrane, probably through the generation of ROS [36]. To examine this possibility, we added the lipoplex to ECV304 cells, a cell line possessing endothelial cell-like characteristics. We found that the lipoplex induced the production of a significant amount of intracellular ROS. These results suggest two possible pathways of NF-κB activation in the lung after *in vivo* lipofection: (1) NF-κB is directly activated by the lipoplex accumulated in the lung through ROS production and (2) NF-κB undergoes secondary activation by TNF-α in the circulation induced by lipofection. The previous study reported that pulmonary capillary endothelial cells appear to be more efficient at the nuclear transfer or gene expression process than the pulmonary epithelial cells after intravenous injection of a lipoplex [37]. In addition, activation of NF-κB by LPS or other stimuli has been demonstrated in cultured endothelial cells using EMSA [38]. Therefore, it is reasonable to speculate that the endothelial cells in the lung are the cells in which transgene expression as well as NF-κB activation take place after administration of lipoplex.

Tan *et al.* [21] previously reported that systemically produced TNF-α reduces transfection efficiency in the lung after *in vivo* lipofection. However, here we have shown that increased transgene expression was obtained after intravenous administration of LPS (Figure 3), during which a significant amount of TNF-α was secreted (data not shown). A possible explanation for this phenomenon

is that the CMV promoter is activated by NF-κB that has been activated by LPS-induced TNF-α [15,16]. The CMV promoter contains 4 repeats of NF-κB-binding sequences, which enable these two to interact with each other [33]. In Figure 2, significant activation of NF-κB was observed after intravenous administration of LPS (lane 4). In addition, the binding of NF-κB to pCMV-Luc was clearly demonstrated (Figure 2, lane 6). These findings support the experimental results showing that transgene expression by pCMV-Luc is positively correlated with the level of NF-κB activation in the lung. Observations from other studies also support these findings: CMV promoter activity was induced by inflammation in the rat arthritis model, where a positive correlation between transgene expression and the dose of LPS was obtained [39]. Reactivation of the previously silenced CMV promoter was observed after administration of LPS in mouse liver [40]. Finally, γ-irradiation enhanced transgene expression in leukemic cells only when a gene of interest was under the control of a CMV promoter [41]. Considering these previous observations and the current experimental finding that transgene expression and NF-κB activation in the lung are positively correlated (Figures 2 and 3), it is suggested that NF-κB activation plays an important role in transgene expression produced by lipofection.

Based on these findings, we hypothesized that transgene expression by lipofection can be enhanced by utilization of activated NF-κB. LPS cannot be used to activate NF-κB for practical situations because of its pyrogenic property. Instead, we constructed a novel plasmid DNA, pCMV-κB-Luc, by inserting 5 serial repeats of NF-κB-binding sequences upstream of the CMV promoter in pCMV-Luc. The competitive EMSA clearly demonstrated that insertion of the NF-κB-binding sequences can enhance the probability of interaction between NF-κB and plasmid DNA. As a result, the pCMV-κB-Luc-containing lipoplex showed a significantly greater transgene expression than that with pCMV-Luc in the lung (Figure 4A), as well as in cultured cells (Figure 5). Plasmid DNA should dissociate from the lipoplex to interact with activated NF-κB through its NF-κB-binding sequence. As shown in previous studies [42–44], plasmid DNA can be released from the lipoplex and the DNA released is transported into the nucleus. Therefore, any approach to facilitate the dissociation, such as the addition of polyethylene-glycol-modified ceramides into liposomes [45], may further improve the NF-κB-dependent increase in transgene expression by pCMV-κB-Luc. This enhanced transgene expression was probably achieved through an increased translocation of plasmid DNA into the nucleus by using the NLS of NF-κB, as suggested in a previous report [34]. The competitive EMSA would support this hypothesis (Figure 7).

Another explanation for the enhanced transgene expression is that the inserted NF-κB-binding sequences act as enhancers and directly upregulate the transcription of luciferase. However, this possibility is unlikely because of our data showing that gene transfer to the lung and liver following a naked pCMV-κB-Luc injection, where NF-κB was hardly activated, gave identical transgene expression to that obtained by a naked pCMV-Luc (Figures 4B and 4C). Tan *et al.* reported that co-injection of phosphorothioate oligonucleotides containing an NF-κB-binding sequence (NF-κB decoy) with lipoplex increased transgene expression in the lung [46]. Therefore, the inserted NF-κB-binding sequence may function as a molecular decoy for NF-κB, which could reduce NF-κB activation in the lung. However, stable oligonucleotides at high doses were required to reduce NF-κB activation [46], suggesting that the short NF-κB-binding sequence in the pCMV-κB-Luc will not act as a NF-κB decoy.

In conclusion, we clearly demonstrated that NF-κB in the lung is activated by an intravenous injection of the lipoplex. There was a positive correlation between transgene expression and NF-κB activation. Finally, we succeeded in constructing a novel and potent plasmid DNA with additional NF-κB-binding sequences that efficiently uses the NF-κB activated by the lipoplex to enhance transgene expression. These findings offer a novel strategy whereby a vector is designed to use the biological response against the vector itself. A better understanding of biological responses against various gene transfer approaches will provide us with useful information for designing a novel and potent approach to effective *in vivo* gene transfer.

Acknowledgements

This work was supported in part by Grants-In-Aid for Scientific Research from the Ministry of Education, Culture, Sports, Science and Technology, Japan, and by grants from the Ministry of Health, Labour and Welfare, Japan.

References

1. Luo D, Saltzman WM. Synthetic DNA delivery system. *Nat Biotechnol* 2000; **18**: 33–37.
2. Felgner PL. Nonviral strategies for gene therapy. *Sci Am* 1997; **276**: 102–106.
3. Felgner PL, Gadek TR, Holm M, *et al.* Lipofection: a highly efficient, lipid-mediated DNA-transfection procedure. *Proc Natl Acad Sci U S A* 1987; **84**: 7413–7417.
4. Subramanian A, Ranganathan P, Diamond SL. Nuclear targeting peptides for lipofection of nondividing mammalian cells. *Nat Biotechnol* 1999; **17**: 873–877.
5. Zabner J, Fasbender AJ, Moninger T, *et al.* Cellular and molecular barriers to gene transfer by a cationic lipid. *J Biol Chem* 1995; **270**: 18 997–19 007.
6. Sakurai F, Nishioka T, Saito H, *et al.* Interaction between DNA-cationic liposome complexes and erythrocytes is an important factor in systemic gene transfer via the intravenous route in mice: the role of the neutral helper lipid. *Gene Ther* 2001; **8**: 677–686.
7. Whitmore M, Li S, Huang L. LPD lipopolyplex initiates a potent cytokine response and inhibit tumor growth. *Gene Ther* 1999; **6**: 1867–1875.
8. Klinman DM, Yi AK, Beaucage SL, *et al.* CpG motifs present in bacterial DNA rapidly induce lymphocytes to secrete interleukin 6, interleukin 12 and interferon γ. *Proc Natl Acad Sci U S A* 1996; **93**: 2879–2883.
9. Krieg AM, Yi AK, Matson S, *et al.* CpG motifs in bacterial DNA trigger direct B cell activation. *Nature* 1995; **374**: 546–549.

10. Sakurai F, Terada T, Yasuda K, *et al.* The role of tissue macrophages in the induction of proinflammatory cytokine production following intravenous injection of lipoplexes. *Gene Ther* 2002; **9**: 1120–1126.
11. Yew NS, Zhao H, Wu IH, *et al.* Reduced inflammatory response to plasmid DNA vectors by elimination and inhibition of immunostimulatory CpG motifs. *Mol Ther* 2000; **1**: 255–262.
12. Hofman CR, Dileo JP, Li Z, *et al.* Efficient in vivo gene transfer by PCR amplified fragment with reduced inflammatory activity. *Gene Ther* 2001; **8**: 71–74.
13. Tan Y, Liu F, Li Z, *et al.* Sequential injection of cationic liposome and plasmid DNA effectively transfects the lung with minimal inflammatory toxicity. *Mol Ther* 2001; **3**: 673–682.
14. Lowenthal JW, Ballard DW, Bohnlein E, *et al.* Tumor necrosis factor alpha induces proteins that bind specifically to κB-like enhancer elements and regulate interleukin 2 receptor α-chain gene expression in primary human T lymphocytes. *Proc Natl Acad Sci U S A* 1989; **86**: 2331–2335.
15. Pahl HL. Activators and target genes of Rel/NF-κB transcription factors. *Oncogene* 1999; **18**: 6853–6866.
16. Karin M, Neriah YB. Phosphorylation meets ubiquitination: the control of NF-κB activity. *Ann Rev Immunol* 2000; **18**: 621–663.
17. Sha WC, Liou HC, Tuomanen EI, *et al.* Targeted disruption of the p50 subunit of NF-κB leads to multifocal defects in immune responses. *Cell* 1995; **80**: 321–330.
18. Griffin GE, Leung K, Folks TM, *et al.* Activation of HIV gene expression during monocyte differentiation by induction of NF-κB. *Nature* 1989; **339**: 70–73.
19. Nishikawa M, Nakano T, Okabe T, *et al.* Residualizing indium-111-radiolabel for plasmid DNA and its application to tissue distribution study. *Bioconjugate Chem* 2003; **14**: 955–961.
20. Liu F, Song Y, Liu D. Hydrodynamics-based transfection in animals by systemic administration of plasmid DNA. *Gene Ther* 1999; **6**: 1258–1266.
21. Tan Y, Li S, Pitt BR, *et al.* The inhibitory role of CpG immunostimulatory motifs in cationic lipid vector-mediated transgene expression in vivo. *Hum Gene Ther* 1999; **10**: 2153–2161.
22. Unlap M, Jope RS. Dexamethasone attenuates NF-κB binding activity without inducing IκB level in rat brain in vivo. *Mol Brain Res* 1997; **45**: 83–89.
23. Zhou D, Brown SA, Yu T, *et al.* High dose of ionizing radiation induced tissue-specific activation of nuclear factor-κB in vivo. *Radiat Res* 1999; **151**: 703–709.
24. Tripp CA, Wolf SF, Unanue ER. Interleukin 12 and tumor necrosis factor α are costimulators of interferon γ production by natural killer cells in severe combined immunodeficiency mice with listeriosis, and interleukin 10 is a physiologic antagonist. *Proc Natl Acad Sci U S A* 1993; **90**: 3725–3729.
25. Liu Y, Mounkes LC, Liggitt HD, *et al.* Factors influencing the efficiency of cationic liposome-mediated intravenous gene delivery. *Nat Biotechnol* 1997; **15**: 167–173.
26. Mahato RI, Kawabata K, Nomura T, *et al.* Physicochemical and pharmacokinetic characteristics of plasmid DNA/cationic liposome complexes. *J Pharm Sci* 1995; **84**: 1267–1271.
27. Nishikawa M, Huang L. Nonviral vectors in the new millennium: delivery barriers in gene transfer. *Hum Gene Ther* 2001; **12**: 861–870.
28. Templeton NS, Lasic DD, Frederik PM, *et al.* Improved DNA : liposome complexes for increased systemic delivery and gene expression. *Nat Biotechnol* 1997; **15**: 167–173.
29. Ren T, Song YK, Zhang G, *et al.* Structural basis of DOTMA for its high intravenous transfection activity in mouse. *Gene Ther* 2000; **7**: 764–768.
30. Ohno M, Fornerod M, Mattaj IW. Nucleocytoplasmic transport: the last 200 nanometers. *Cell* 1998; **92**: 327–336.
31. Dean DA. Import of plasmid DNA into the nucleus is sequence specific. *Exp Cell Res* 1997; **230**: 293–301.
32. Dean DA, Dean BS, Muller S, *et al.* Sequence requirements for plasmid nuclear import. *Exp Cell Res* 1999; **253**: 713–722.
33. Assogba BD, Choi BH, Rho HM. Transcriptional activation of the promoter of human cytomegalovirus immediate early gene (CMV-IE) by the hepatitis B viral X protein (HBx) through the NF-κB site. *Virus Res* 2002; **84**: 171–179.
34. Mesika A, Grigoreva I, Zohar M, *et al.* A regulated, NFκB-assisted import of plasmid DNA into mammalian cell nuclei. *Mol Ther* 2001; **3**: 653–657.
35. Sakurai F, Nishioka T, Yamashita F, *et al.* Effects of erythrocytes and serum proteins on lung accumulation of lipoplexes containing cholesterol or DOPE as a helper lipid in the single-pass rat lung perfusion system. *Eur J Pharm Biopharm* 2001; **52**: 165–172.
36. Aramaki Y, Takano S, Tsuchiya S. Cationic liposomes induce macrophage apoptosis through mitochondrial pathway. *Arch Biochem Biophys* 2000; **392**: 245–250.
37. McLean JW, Fox EA, Baluk P, *et al.* Organ-specific endothelial cell uptake of cationic liposome–DNA complexes in mice. *Am J Physiol Heart Circ Physiol* 1997; **273**: H387–404.
38. Deshpande D, Blezinger P, Pillai R, *et al.* Target specific optimization of cationic lipid-based systems for pulmonary gene therapy. *Pharm Res* 1998; **15**: 1340–1347.
39. Pan RY, Xiao X, Chen SL, *et al.* Disease-inducible transgene expression from a recombinant adeno-associated virus vector in a rat arthritis model. *J Virol* 1999; **73**: 3410–3417.
40. Loser P, Jennings GS, Strauss M, *et al.* Reactivation of the previously silenced cytomegalovirus major immediate early promoter in the mouse liver: involvement of NFκB. *J Virol* 1998; **72**: 180–190.
41. Vereecque R, Saudemont A, Wickham TJ, *et al.* γ-Irradiation enhances transgene expression in leukemic cells. *Gene Ther* 2003; **10**: 227–233.
42. Almoftia MR, Harashimab H, Shinoharaa Y, *et al.* Cationic liposome-mediated gene delivery: Biophysical study and mechanism of internalization. *Arch Biochem Biophys* 2003; **410**: 246–253.
43. Xu Y, Szoka FC Jr. Mechanism of DNA release from cationic liposome/DNA complexes used in cell transfection. *Biochemistry* 1996; **35**: 5616–5623.
44. Zabner J, Fasbender AJ, Moninger T, *et al.* Cellular and molecular barriers to gene transfer by a cationic lipid. *J Biol Chem* 1995; **270**: 18 997–19 007.
45. Shi F, Wasungu L, Nomden A, *et al.* Interference of poly(ethylene glycol)–lipid analogues with cationic-lipid-mediated delivery of oligonucleotides; role of lipid exchangeability and non-lamellar transitions. *Biochem J* 2002; **366**: 333–341.
46. Tan Y, Zhang JS, Huang L. Codelivery of NF-κB decoy-related oligodeoxynucleotide improves LPD-mediated systemic gene transfer. *Mol Ther* 2002; **6**: 804–812.

Available online at www.sciencedirect.com

SCIENCE DIRECT®

Advanced Drug Delivery Reviews 57 (2005) 675–688

Advanced DRUG DELIVERY Reviews

www.elsevier.com/locate/addr

Theoretical considerations involving the pharmacokinetics of plasmid DNA

Makiya Nishikawa[a,*], Yoshinobu Takakura[a], Mitsuru Hashida[b]

[a]*Department of Biopharmaceutics and Drug Metabolism, Graduate School of Pharmaceutical Sciences, Kyoto University, Sakyo-ku, Kyoto 606-8501, Japan*

[b]*Department of Drug Delivery Research, Graduate School of Pharmaceutical Sciences, Kyoto University, Sakyo-ku, Kyoto 606-8501, Japan*

Received 6 March 2004; accepted 18 December 2004

Abstract

Success of in vivo gene therapy relies on the development of gene delivery technologies, by which a well-controlled transgene expression is achieved as far as the spatial and temporal profile of the expression is concerned. Because transgene expression only occurs in cells that are transduced with the gene administered, the tissue distribution of genes is an important factor determining the efficacy of in vivo gene transfer. Plasmid DNA is the simplest vector and its administration in naked or complexed form results in significant transgene expression in various organs. The route of administration, the use of cationic vectors and the administration technique greatly affects the tissue distribution of plasmid DNA and the subsequent transgene expression. Therefore, a clear understanding of the tissue distribution of naked and complexed plasmid DNA is a prerequisite for strategies for developing effective in vivo gene transfer methods. Pharmacokinetics translates the tissue distribution properties of plasmid DNA into quantitative parameters, which can be compared with parameters obtained under different conditions, or with physiological parameters such as blood flow rate. Here we discuss the pharmacokinetic evaluation of the tissue distribution characteristics of plasmid DNA, in the free and complexed forms.

Keywords: Gene transfer; Tissue distribution; Clearance; Receptor-mediated endocytosis

Contents

* Corresponding author. Tel.: +81 75 753 4616; fax: +81 75 753 4614.
E-mail address: makiya@pharm.kyoto-u.ac.jp (M. Nishikawa).

0169-409X/$ - see front matter © 2005 Elsevier B.V. All rights reserved.
doi:10.1016/j.addr.2004.12.003

1. Introduction

In vivo gene replacement therapy requires the development of gene delivery technologies, by which a well-controlled transgene expression is achieved as far as the spatial and temporal profile of the expression is concerned. Although genes can be easily introduced to cells ex vivo by means of viruses, cationic liposomes (lipids) or electric pulses, their administration directly to patients represents an ideal methodology for the treatment of a variety of diseases. Following in vivo administration, however, genes encounter various hurdles that need to be overcome for a successful in vivo gene therapy (Fig. 1).

Transgene expression only occurs in cells that are transduced with the gene administered. Therefore, the tissue distribution of genes is an important factor determining the efficacy of in vivo gene transfer. Generally speaking, the tissue distribution of an externally administered compound is determined by its interaction with the body, and such interaction is regulated by the physicochemical and biological properties of the compound and the anatomical and physiological properties of the body. Therefore, drug targeting depends on optimizing the properties of the drug delivery system [1,2], or by altering the properties of the body. One example of the latter is the osmotic opening of the blood–brain barrier [3]. Theoretically, changing the route of administration, for example intraarterial injection to the target organ instead of intravenous injection, is also a promising approach for improving the targeting efficiency of a drug [4]. Similar strategies could be applied to genes for delivering them to target cells. However, unlike most conventional drugs, genes need to find a way into the intracellular space where they can then exert their effects.

Since Wolff et al. [5] reported that transgene products can be obtained in skeletal muscle by a simple intramuscular injection of naked plasmid DNA, it is now widely accepted that plasmid DNA is a promising nonviral vector for in vivo gene transfer. Even for systemic administration, naked plasmid DNA can produce high levels of transgene product when it is rapidly injected into the systemic circulation in a large-volume solution [6]. However, a conventional intravenous injection of plasmid DNA results in undetectable transgene expression in major organs [7,8]. Altered tissue and intracellular distribution of plasmid DNA would explain such differences in the final outcome of transgene expression (see the review by Kobayashi et al. [9] in this issue). To improve the delivery and cellular uptake of plasmid DNA after in vivo administration, a number of cationic delivery systems have been developed. Plasmid DNA forms electrostatic complexes with these cationic vectors and, within the body, such complexes interact with various components and show complicated distribution profiles.

A clear understanding of the tissue distribution of plasmid DNA and its complexes with nonviral vectors is a prerequisite for a strategy for developing novel in vivo gene transfer methods. Pharmacokinetics translates the tissue distribution properties of plasmid DNA into quantitative parameters, which can be compared with parameters obtained under different conditions, or with physiological parameters such as blood flow rate and the rate of fluid-phase endocytosis. Here, we discuss the pharmacokinetics of the tissue distribution characteristics of plasmid DNA, which is systemically

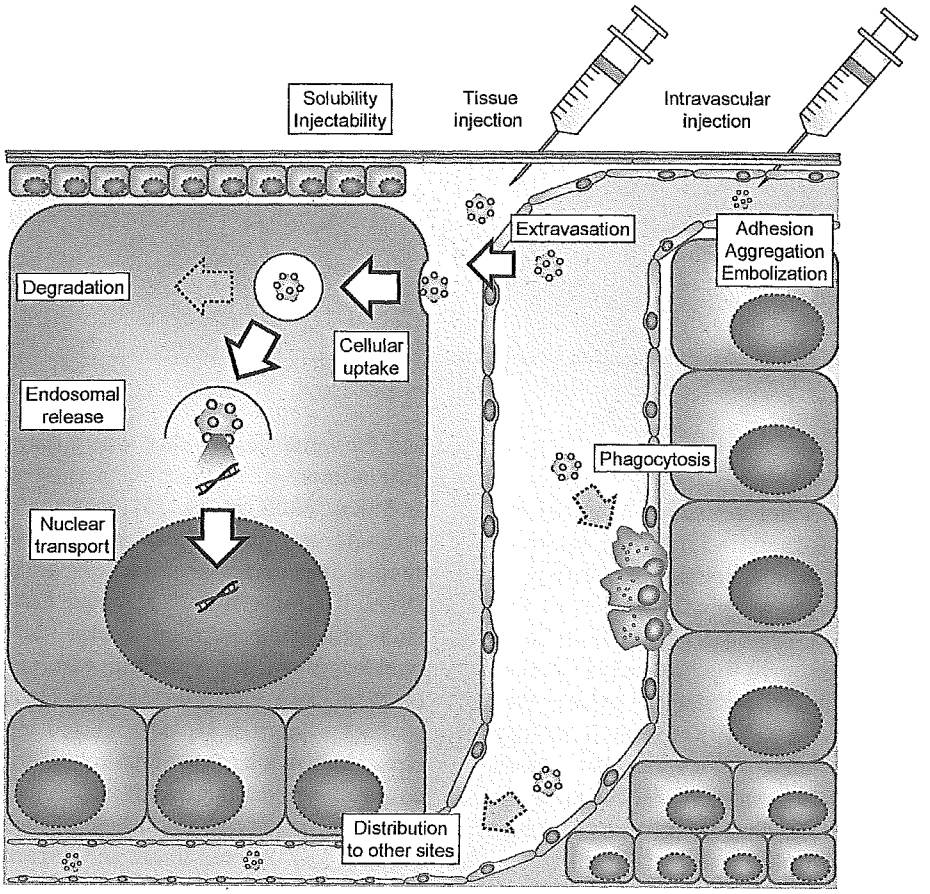

Fig. 1. Hurdles in gene delivery following in vivo administration. The vector system should be soluble and injectable, avoid adhesion (non-specific binding) to tissues, aggregation, embolization, and phagocytosis, extravasate, find a way to the inside of target cell, escape from endosomal/lysosomal degradation, and be transported into the nucleus. When any vector or delivery system is used for the delivery of plasmid DNA, the DNA should be released prior to the nuclear entry.

administered in the free and complexed forms. Because plasmid DNA possesses several features common to other macromolecular compounds in terms of tissue distribution, the pharmacokinetic characteristics of macromolecules are first summarized. Cell-specific delivery approaches that have been applied to targeted gene delivery are also evaluated in pharmacokinetic terms.

2. Pharmacokinetic analysis of tissue distribution characteristics of macromolecules

Although, if not protected, plasmid DNA is easily degraded by nucleases following administration, fractions maintaining the structure could behave as macromolecules in vivo. Therefore, it is important to summarize the factors determining the tissue distribution characteristics of macromolecules. Pharmacokinetic analysis based on the concept of clearance is used to quantitatively evaluate the determinants affecting the tissue distribution of macromolecules.

2.1. Theoretical background of the analysis

2.1.1. Uptake by target

The tissue distribution of a macromolecule via the circulation can be pharmacokinetically analyzed based on the concept of clearance. Tissue uptake

of a macromolecule consists of uptake from the plasma and efflux from the tissue. When the tissue uptake rate is assumed to be independent of its concentration in the plasma and the efflux process follows first-order rate kinetics, the change in its amount in a tissue with time can be described as follows:

$$\frac{dX_i}{dt} = CL_{app,i}C_p - k_{efflux,i}X_i \quad (1)$$

where X_i (μg) represents an amount of the macromolecule in tissue i after administration, C_p (μg/ml) is its concentration in the plasma, $CL_{app,i}$ (ml/h) expresses the apparent tissue uptake clearance from the plasma to tissue i, and $k_{efflux,i}$ (h^{-1}) represents the efflux rate from tissue i.

An assumption of negligible efflux from the tissue ($k_{efflux,i}$=0) makes it easier to pharmacokinetically analyze the distribution process of macromolecules. Macromolecular drugs, such as proteins and plasmid DNA, are labile to undergo degradation before and after cellular uptake. When traced with radioisotopes, radioactive metabolites are sometimes rapidly released from the cells that have taken up the radiolabeled compound. This is the case when galactosylated bovine serum albumin (Gal-BSA), a macromolecular ligand for the asialoglycoprotein receptors on hepatocytes [10,11], undergoes direct ^{125}I radiolabeling on the tyrosine residues. Fig. 2A shows the radioactivity in mouse liver after intravenous injection of Gal-BSA labeled with ^{125}I or ^{111}In [12]. Upon administration, Gal-BSA is rapidly taken up by the liver via the asialoglycoprotein receptor-mediated endocytosis. The endocytosed material is degraded within the lysosomes [13,14], which leads to the release of radioactive metabolites from the liver. This release makes it difficult to estimate the uptake clearance by the liver. On the other hand, little radioactivity was released from the liver during the experimental period when Gal-BSA was labeled with ^{111}In using diethylenetriaminepentaacetic dianhydride as a chelating agent (Fig. 2A). The physicochemical properties of radioactive metabolites will explain such differences [15], and 'residualizing' radiolabels which support the assumption that there is little efflux from tissues after uptake have been investigated for radioiodine [16–18] and metallic chelates [19–21]. These results indicate that if a macromolecule is labeled by a proper method, the efflux process in the pharmacokinetic analysis can be ignored even though the compound itself undergoes intracellular degradation. Based on these considerations, we recently developed a residualizing radiolabel for plasmid DNA [22]. Compared with its ^{32}P-labeled counterpart, ^{111}In-labeled naked plasmid DNA showed a prolonged retention of radioactivity in the liver after intravenous injection in mice (Fig. 2B).

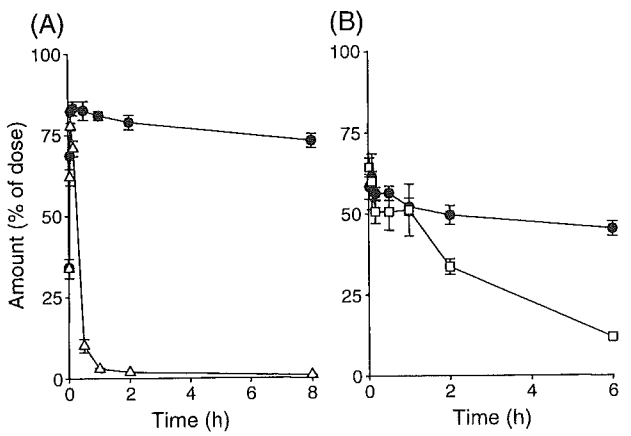

Fig. 2. Time courses of radioactivity in the liver after intravenous injection of (A) galactosylated bovine serum albumin (Gal-BSA) or (B) plasmid DNA in mice after intravenous injection. Data are expressed as the mean±S.D. of three mice. (A) ●, ^{111}In-Gal-BSA; △, ^{125}I-Gal-BSA. (B) ●, ^{111}In-plasmid DNA; □, ^{32}P-plasmid DNA.

Under the assumption of negligible efflux from the tissue, Eq. (1) is simplified to:

$$\frac{dX_i}{dt} = CL_{app,i}C_p \quad (2)$$

Integration of Eq. (2) from time 0 to t_1 gives:

$$CL_{app,i} = \frac{X_{i,t_1}}{\int_0^{t_1} C_p dt} = \frac{X_{i,t_1}}{AUC_{p,0-t_1}} \quad (3)$$

where AUC_p (μg h/ml) is the area under the plasma concentration–time curve of the macromolecule. Its elimination profile from the plasma can be expressed as a function of one or more exponentials in many cases. Then, the AUC_p values at any time point can be calculated by fitting an equation to the experimental data using a least-squares method. According to Eq. (3), $CL_{app,i}$ is calculated from the slope of the plot of the amounts in the tissue (X_i) against AUC_p. Table 1 summarizes the AUC and clearances of several model macromolecules in mice after intravenous injection; these parameters clearly indicate that the tissue distribution characteristics of macromolecules are dependent on parameters, such as the molecular weight and electric charge as discussed below.

Tissue uptake clearances are useful parameters for characterizing the tissue distribution properties of a macromolecule because they are independent on its concentration in the plasma. However, the tissue uptake process sometimes depends on its concentration in plasma and follows non-linear kinetics. Then, the calculated $CL_{app,i}$ would represent an average value of its time-dependent clearances for the overall experimental period [10].

$CL_{app,i}$ is a hybrid parameter of the plasma flow rate (Q, ml/h) to the tissue and the intrinsic uptake clearance ($CL_{int,i}$) by the tissue. Therefore, it can be expressed as:

$$CL_{app,i} = \frac{QCL_{int,i}}{Q + CL_{int,i}} \quad (4)$$

This equation clearly demonstrates the limitation of gene delivery to tissues with a low blood flow rate; if $CL_{int,i}$ is successfully increased by any means, $CL_{app,i}$ approaches to Q. Table 2 summarizes the blood flow rate to various tissues in human [23]. Compared with the rate normalized for tissue weight, the blood flow to the kidney, liver, and brain is much higher than that to the skin, muscle, and fat. Therefore, even although skeletal muscle is an important target for in vivo gene transfer, it is difficult to deliver plasmid DNA to the

Table 1
AUC and clearances of model macromolecules in mice after intravenous injection

Compound	Molecular weight (kDa)	Charge, ligand	Dose (mg/kg)	AUC (%dose h/ml)	CL_{total}	$CL_{app,liver}$	CL_{urine}
^{111}In-plasmid DNA	~4000	Strongly anionic	0.5	2.8	36.0	17.8	–
^{111}In-Suc_{40}-BSA	70	Strongly anionic	0.1	1.5	64.9	48.0	0.17
^{14}C-dextran sulfate	8	Strongly anionic	1	4.0	25.3	2.47	12.3
^{3}H-oligo DNA	3	Strongly anionic	1	1.3	75.0	11.1	17.0
^{111}In-BSA	67	Anionic	1	1430	0.07	0.02	0.01
^{14}C-CM-dextran	70	Anionic	100	1010	0.10	0.01	0.07
^{14}C-dextran	70	Neutral	100	146	0.69	0.24	0.26
^{14}C-dextran	10	Neutral	100	6.6	15.2	0.24	12.8
^{14}C-DEAE-dextran	70	Cationic	100	51	1.96	0.36	1.06
^{111}In-PLL	60	Cationic	1	0.6	159	66.1	0.32
^{111}In-Cat-BSA	70	Cationic	1	2.8	35.5	24.8	0.40
^{111}In-Gal_{36}-BSA	70	Anionic, Gal	0.1	1.2	85.0	77.3	0.16
^{111}In-Man_{16}-BSA	70	Anionic, Man	0.1	5.0	20.0	14.3	n.d.
^{111}In-Gal_{28}-PLL	60	Cationic, Gal	1	0.6	175	97.1	0.19

BSA, bovine serum albumin; Suc-, succinylated; CM-dextran, carboxymethyl-dextran; DEAE-dextran, diethylaminoethyl-dextran; PLL, poly-L-lysine; Cat-, cationized; Gal-, galactosylated; Man-, mannosylated. n.d., not determined. These data are cited from our previous studies [2,11,22,36,40,80].

Table 2
Human tissue volume and blood flow rate to tissues [23]

Tissue	Male			Female		
	Volume (ml)	Flow (ml/min)	Perfusion rate (ml/min/ml)	Volume (ml)	Flow (ml/min)	Perfusion rate (ml/min/ml)
Brain	1400	720	0.51	1200	624	0.52
Kidneys	310	1140	3.68	275	884	3.22
Liver	1800	(1500)	(0.84)	1400	(1404)	(1.00)
Arterial		390	0.22		338	0.24
Portal		1110	0.62		1066	0.76
Muscle	30000	1020	0.03	18000	624	0.03
Fat	12500	300	0.02	17500	442	0.03
Subcutaneous	7500			13000		
Other	5000			4500		
Heart: without blood	330	240	0.73	270	260	0.96
Skin	(2600)	300	0.12	(1790)	260	0.15
Epidermis	100			90		
Dermis	2500			1700		
Splanchnic	(1480)	(1140)	–	(1365)	(1092)	–
Pancreas	100	60	0.60	85	52	0.61
Spleen	180	180	1.00	150	156	1.04
GI tract	(1200)	(900)	–	(1130)	(884)	–
Stomach	150	60	0.32	140	52	0.31
Intestine	(1010)	(840)	–	(960)	(832)	–
Small	640	600	0.94	600	572	0.95
Large	370	240	0.65	360	260	0.72
Skeleton	10500	300	0.03	8500	260	0.03
Remainder	4936	355	–	4291	328	–
Total	73000	6000	–	60000	5200	–

organ via the vascular route under a normal conditions. To overcome this limitation, improvement in administration techniques is needed. Efficient delivery of plasmid DNA to skeletal muscle or the diaphragm muscle has been successfully achieved by temporally restricting the distribution of plasmid DNA only to the target tissue [24–26].

2.1.2. Balance of the clearances of target and non-target tissues

The total body clearance (CL_{total}, ml/h) of a macromolecule can be calculated using AUC_p for infinite time ($AUC_{p,\infty}$) and the dose (D) as follows:

$$CL_{total} = \frac{D}{AUC_{p,\infty}} \quad (5)$$

Because CL_{total} can be considered as the sum of CL_{target} (the uptake clearance of the target tissue), $CL_{non\text{-}target}$ and the degradation clearance within the systemic circulation (CL_{deg}), the fraction of the macromolecule delivered to the target (F_{target}) can be calculated as:

$$F_{target} = \frac{CL_{target}}{CL_{total}} = \frac{CL_{target}}{CL_{target} + CL_{non-target} + CL_{deg}} \quad (6)$$

Therefore, the potential of the targeted delivery of plasmid DNA can be quantitatively explained by the parameters of CL_{target}, $CL_{non\text{-}target}$, and CL_{deg}. Eq. (6) clearly indicates that an approach increasing the CL_{target} and/or reducing the $CL_{non\text{-}target}$ or CL_{deg} of plasmid DNA is suitable for achieving an efficient gene transfer at the target site.

2.2. Anatomical and physiological properties of the body

Macromolecules entering the systemic circulation distribute to tissues largely via the bloodstream. Therefore, as discussed above, the blood flow rate

determines the delivery rate of macromolecules to each tissue.

Macromolecules in the circulation have a direct access to the capillary endothelial cells as well as various circulating cells in the blood. These cells have the opportunity to take up macromolecules via specific or nonspecific interactions. The interaction of macromolecules with parenchymal cells in tissues can occur only when they have access through the endothelial lining. The structure of the blood capillary wall varies greatly depending on the organ. In addition, pathological states such as inflammation could change the structure. On the basis of the morphology and continuity of the endothelial layer and the basement membrane, the capillary endothelium can be divided into the continuous, fenestrated and discontinuous endothelium [27,28].

Tight junctions between endothelial cells and underlying uninterrupted basement membrane characterize the continuous endothelium, through which the passage of macromolecules is greatly restricted. This type of endothelium can be found in skeletal, cardiac, and smooth muscles, and in lung, skin, and subcutaneous tissues. Macromolecules of around 6 nm in diameter or more hardly interact with parenchymal cells in these tissues simply due to the barrier posed by the endothelium. Endothelial cells having fenestrae equipped with a diaphragm, an opening 40–80 nm in diameter, form the fenestrated endothelium in the intestinal mucosa, the endocrine and exocrine glands, and the glomerulus and peritubules of the kidney. However, the passage of macromolecules through this type of endothelium is limited by the presence of the basement membrane. A clear relationship between the molecular weight and glomerular filtration has been reported using dextrans [29] and other macromolecules [30]; macromolecules with a molecular weight of 40 kDa or more are scarcely excreted into the urine. Discontinuous or sinusoidal endothelium is found only in the liver, spleen, and bone marrow. These capillaries are characterized by endothelial gaps, intercellular junctions with a diameter up to 30–500 nm and with either no basement membrane (liver) or a discontinuous basement membrane (spleen and bone marrow). Therefore, parenchymal cells in these tissues can be accessed by macromolecules with relatively high molecular weight. Enhanced vascular permeability of macromolecules is also found in solid tumors [31].

2.3. Physicochemical properties of macromolecules

Depending on the anatomical and physiological properties of tissues, macromolecules are delivered to the vicinity of various cells in the body. Then, they interact with some of those cells depending on their physicochemical properties. The summation of such interactions determines the overall pharmacokinetics of each macromolecule. The physicochemical properties such as the size, charge, and specific structures recognized by any specific molecule on cell surface govern the interaction; this is the basis of designing a drug delivery system. Understanding the effects of the physicochemical properties of macromolecules on their tissue distribution allows us to theoretically design delivery systems not only for drugs but also for genes.

Because the passage through the endothelial cells is strictly regulated by size, the molecular weight of macromolecules greatly affects their tissue distribution. Macromolecules with a molecular weight of about 40 kDa or less pass through the renal glomerular capillary wall [29,30,32,33], resulting in a short plasma half-life. Oligonucleotides with a molecular weight less than the threshold undergo rapid glomerular filtration by the kidney [34,35]. Plasmid DNA, on the other hand, is too large to be filtered without degradation.

Another important characteristic of macromolecules is their electric charge. Because the cell surface is negatively charged, cationic molecules tend to electrostatically bind to it, resulting in greater tissue uptake. Although cationic macromolecules might bind to any type of cells in vivo, they are mainly delivered to the liver, kidney, or lung after intravenous administration. Cationic plasmid DNA complexes are generally trapped by the lung, which could be due to the direct interaction between cationic complexes and the endothelial cells in the lung, or to the embolization of aggregates of such complexes with blood components as discussed below. Neutral or weakly anionic macromolecules, such as polyethylene glycol and serum albumin, possess a very weak affinity for the cell surface, so they are cleared very slowly if the molecular size exceeds the threshold of the glomerular

filtration. A further reduction in the charge of the macromolecules, on the other hand, increases the affinity for cells having specific receptors that can be categorized as scavenger receptors [36].

2.4. Interaction with blood components

Although macromolecules distribute within the body depending on their physicochemical properties, the interaction with blood components is another factor regulating their tissue distribution [23].

Particulate carriers such as cationic liposomes that are used as nonviral vectors attract a number of serum proteins [37]. It has also been reported that the type and amount of serum proteins bound to the surface in part controls the tissue distribution of particulate carriers [38,39]. Some macromolecules can also interact with blood components. We have shown that mannan binding proteins in serum can bind to mannosylated macromolecules and alter their tissue distribution [40].

Blood cells also contribute to the interaction of cationic plasmid DNA complexes after intravenous injection. Sakurai et al. [41,42] reported that some plasmid DNA complexes with cationic liposomes bind to erythrocytes, form large aggregates and are captured by the lung capillaries.

2.5. Receptor-mediated uptake

Active targeting of genes will increase the therapeutic efficacy and reduced the potential side effects of in vivo gene therapy. Therefore, various approaches have been investigated to achieve targeting, such as the use of monoclonal antibodies or ligands for cell-surface receptors. Because of the cell-specificity of the expression, abundance, and other factors discussed above, receptors for transferrin, asialoglycoproteins, and mannose are the most common receptors that have been used in the targeted delivery of drugs and genes.

Theoretically, the use of a ligand for a receptor increases the uptake clearance of the target tissue, which leads to an increase in F_{target} in Eq. (6). This is the case when BSA, a model macromolecule, is modified with galactose or mannose [11,40]. Although receptor-mediated uptake is a capacity-limited process, the tissue distribution of galactosylated or mannosylated macromolecules can be analyzed using clearances calculated from Eq. (3); then the calculated value represents an average value of the time-dependent (concentration-dependent) clearances of ligands for the overall experimental period. In the case of the asialoglycoprotein receptor–ligand interaction, the binding affinity of the ligand is determined by the clustering and geometric organization of galactose, the number of galactose moieties, and so on. The effects of the number of galactose moieties on the macromolecules were clearly demonstrated by using poly-L-glutamic acid (PLGA) and BSA [11,43]. An increase in the number of galactose moieties increased the $CL_{app,liver}$, because hepatocytes in the liver only express asialoglycoprotein receptors. Because the receptor-mediated uptake of galactosy-

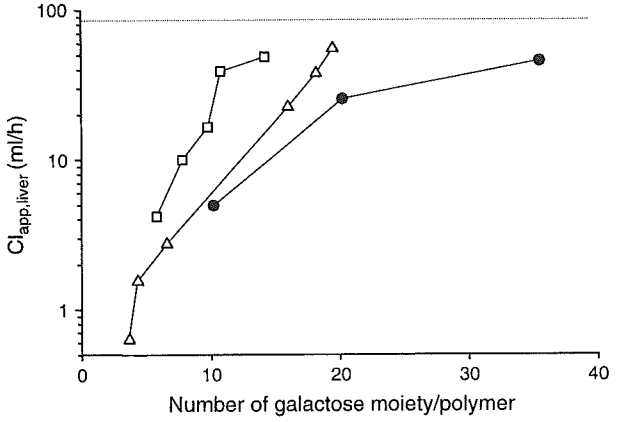

Fig. 3. Apparent hepatic uptake clearances ($CL_{app,liver}$) of galactosylated macromolecules after intravenous injection in mice at a dose of 1 mg/kg. The dashed line represents the plasma flow rate (Q) to the liver in mice. ●, ^{111}In-Gal-BSA; △, ^{111}In-Gal-PLGA, □, ^{111}In-Gal-SOD.

lated macromolecules is so efficient and fast, i.e., the $CL_{int,liver}$ is very large, the $CL_{app,liver}$ approaches to the hepatic plasma flow rate, Q, as the number of galactose moieties increases and the dose administered decreases (Fig. 3).

3. Pharmacokinetics of plasmid DNA following systemic, intravenous administration

Plasmid DNA is a macromolecule with a high molecular weight of about 2500 kDa or more and a strong anionic charge. As discussed above, these properties greatly limit the tissue distribution of plasmid DNA. Without degradation, the large size hinders the access of circulating plasmid DNA to cells except for the blood cells, endothelial cells, and parenchymal cells in the liver and spleen. Some of these cells take up and degrade plasmid DNA, resulting in little transgene expression following a simple intravenous injection of naked plasmid DNA. Cationic molecule-based nonviral vectors are used to increase the affinity of plasmid DNA for cells via electrostatic interaction but, as summarized above, they greatly alter the tissue distribution of plasmid DNA. Several ligands have been used to increase the selectivity of plasmid DNA delivery to target cells. For a very high transgene expression, naked plasmid DNA is injected into mice by the hydrodynamics-based procedure [6].

3.1. Naked DNA

The disappearance of naked plasmid DNA from the blood circulation has been examined in animals using several analytical methods. Houk et al. [44] described the plasma clearance of plasmid DNA after intravenous injection in rats. To detect the structural forms of the DNA, i.e., the supercoiled, open circular, and linear forms, they isolated plasmid DNA from whole blood samples by extraction. Then, the three plasmid DNA forms were separated by gel electrophoresis. They found that the supercoiled plasmid DNA is rapidly metabolized and cleared from the circulation, and is detectable in the bloodstream only after a very high dose of 2500 μg (about 7 mg/kg body weight). Separately, the amount of plasmid DNA in plasma after intravenous injection was also measured by quantitative polymerase chain reaction (PCR) [45]. At a dose of 50 μg to mice, a steady disappearance of the PCR products was observed in serum with a half-life of less than 1 min.

Although these analytical methods are effective in measuring plasmid DNA in solutions like serum, they are not appropriate for evaluating the tissue distribution. Cellular uptake is sometimes combined with a marked degradation of plasmid DNA, which could make it impossible to identify which cells or organs take up the DNA. The most promising alternative is the use of fluorescent- or radio-labeling of plasmid DNA. To date, a number of methods have been developed for studying not only the plasma clearance but also the tissue distribution of plasmid DNA. The most frequently used method for this purpose is ^{32}P-labeling by nick translation. When naked ^{32}P-plasmid DNA was injected as a bolus into the tail vein of mice at a dose of 1 mg/kg, radioactivity rapidly disappeared from plasma and a large fraction (60–70% of the injected dose) was recovered in the liver within 5 min of injection [7]. The pharmacokinetic analysis of the tissue distribution of ^{32}P-plasmid DNA revealed that the $CL_{app,liver}$ is close to the hepatic plasma flow rate, which accounts for a large fraction of the CL_{total}. In a different set of experiments, a rapid degradation in serum was also observed, and the degradation clearance was found to be large enough to digest the DNA with a half-life of less than 10 min. Nonviral vectors would protect the DNA from degradation in the circulation. Under these conditions, naked plasmid DNA resulted in no transgene expression in major organs [8].

Radiolabeling methods account for differences in the tissue distribution data of plasmid DNA. Although $CL_{app,tissue}$ is derived from Eq. (2) under the assumption of negligible efflux of compounds from tissues, the amount of ^{32}P-radioactivity in the liver decreases with time. In addition to ^{32}P-labeling, various methods have been developed to trace the tissue distribution of plasmid DNA. In this regard, radioiodination [46,47], metabolic labeling with ^{3}H-thymidine 5′ -triphosphate [48], or ^{99m}Tc-label [49] have been used to follow the distribution of plasmid DNA in vivo. A number of fluorescence labeling methods are also available to trace the DNA [50–53]. However, the efflux rates of radioactive or fluorescent metabolites are generally too fast, so quantitative pharmacokinetics analyses are difficult to perform using these